

# FIELD-ALIGNED CURRENT DYNAMICS IN TWO SELECTED INTERVALS OF THE 6 APRIL 2000 SUPERSTORM

V.M. Mishin, M.A. Kurikalova, V.V. Mishin (*ISTP SB RAS, Russia*)  
C. Wang, J.Y. Wang (*NSSC CSSAR CAS, Beijing, China*)

**Abstract.** We investigate two intervals of the 2000 April 6 superstorm with the expansion phase (EP) signatures. Obtained were the maps of the field-aligned current (FAC) distribution in the polar ionosphere of the Northern Hemisphere. When analyzing the maps, mesoscale cells with the local maximum of their FAC density in each Iijima and Potemra (I-P) Region were taken into account, which two- or threefold increased the spatial resolution. We describe two EP types (termed "summer" and "winter") for the equinox season. The FAC spatial distribution and dynamics during the expansion phase differ dramatically within these two types. We propose a scenario, in which the winter-type EP starts with the collapse (decrease) of the FAC that flows into the winter hemisphere ionosphere in the R1 premidnight sector. Simultaneously, and almost at the same rate, there occurs the FAC increase in the adjacent R1 postmidnight sector. Thus, in the proposed scenario, the substorm EP starts simultaneously in two hemispheres, but in different MLT-sectors of the nightside I-P Region 1. The magnetosphere-ionosphere (M-I) feedback global instability in the summer hemisphere premidnight sector serves as an initiator and organizer of the global EP.

## 1. Introduction

The paper addresses the common problem of modeling the current system in the disturbed magnetosphere-ionosphere (M-I) system [McPherron *et al.*, 1973; Lui and Kamide, 2003; Akasofu, 2015]. Studying the global distribution and dynamics of field-aligned currents (FACs) also refers to this problem [Weimer, 2001; Papitashvili *et al.*, 2002; Kabin *et al.*, 2004; Korth *et al.*, 2011; Anderson *et al.* 2014]. Versions of modeling electric circuits during substorms [e.g., Lyatsky *et al.*, 1972; Sugiura, 1975; Siscoe, 1982; Kamide and Baumjohann, 1993; Cowley, 2000; Sofko *et al.* 2013; Sandholt *et al.* 2014; Ohtani *et al.*, 2014] have been addressed in the literature. The problem of substorm asymmetry in two hemispheres [Ostgaard *et al.*, 2012; Reistad *et al.* 2014; 2015; Laundal and Ostgaard, 2009] has been also actively investigated. The results of this study are original (see Abstract), but have a direct relation to each of the listed topics.

In this paper, we use the data on the solar wind, AE indices [<http://cdaweb.gsfc.nasa.gov/>], and the data from the global ground-based magnetometer network (see *Acknowledgements*). The latter were processed through the magnetogram inversion technique (MIT-ISTP) [Mishin, 1990]. From the data for the 6 April 2000 two intervals [(02±04) and (12±15) UT], we calculated the time series of the maps for the FAC density distribution in the ionosphere. Kamide and Baumjohann [1993] performed a comparative analysis for different MIT techniques. They noted that the MIT-obtained ionospheric current distribution is not sensitive to the selection of the ionosphere conductivity model, unless the conductivity auroral maximum is displaced in the ionosphere.

Here, we apply the ionosphere conductivity model adapted to the addressed events [Mishin *et al.*, 1986; Shirapov *et al.*, 2000]. One peculiarity of this empirical model is the positive feedback of the computed ionosphere conductivity with the FAC density FAC in the considered point. The other MIT-ISTP peculiarity is the method for choosing an optimal spectrum of the spherical harmonics, whose series approximates the potential of the magnetic field under consideration [Mishin, 1990]. The third feature of this paper is calculating and analyzing the intensities of mesoscale inhomogeneities within the I-P Regions. These original peculiarities of the applied techniques are one of the reasons, why the principal results of this paper have not been obtained in the literature earlier.

Paragraph 2 addresses the technique to determine the FAC intensity within individual ionospheric cells. Paragraphs 3–5 deal with the analysis of temporal series of the maps of the FAC density and intensity distribution in the polar ionosphere during the two selected EP intervals. Paragraph 6 presents discussion and conclusions.

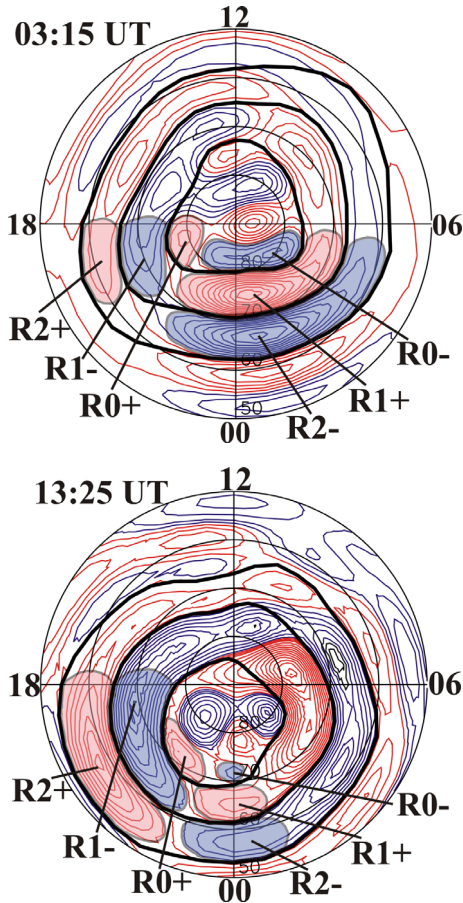
## 2. Determining FAC intensity in cells within every I-P Region

Fig. 1 provides examples of the FAC density distribution maps in corrected geomagnetic coordinates.

Upon determining the boundaries, we find the full FAC value (i.e., FAC intensities) in a cell. To interpret the results and estimate the errors of the operation, we use the schematic model for the electric circuit of the M-I nightside disturbed system in Fig. 2. The model is not identical, but generally it is similar to the known corresponding models [see references in *Introduction*].

In Fig. 2, generator  $G$  is formed in the tail current disruption, and feeds directly the FAC ionospheric cells of Region 1 in two hemispheres. In the Northern Hemisphere, the cells of downward and upward FAC are denoted as  $R1+$  and  $R1-$ . The FAC intensities in these cells are  $I_{R1+}$  and  $I_{R1-}$ . The Region 2 pair [R2+, R2-] and the Region 0

[R0+ and R0-] are connected in parallel to this pair. The ionospheric current from the R1+ FAC cell flows into the R2- and R0- FAC cells, and flows down along field lines into the DRP1 partial ring current.



**Figure 1.** Examples of the FAC density distribution maps: downward (dotted lines) and upward (solid lines) currents. Thick lines are the boundaries of the I-P Regions. Filling shows the highlighted mesoscale cells. We show the boundaries of three I-P Regions [Mishin et al., 2011], as well as the boundaries of mesoscale cells within every Region. The symbols of cells  $R0\pm$ ,  $R1\pm$ ,  $R2\pm$  ( $0,1,2$  is the I-P Region number, the  $+(-)$  sign corresponds to the downward (upward) FAC) are shown for the nightside interval  $\sim(1806)$  UT: it is this interval that is investigated in this paper. There is a local FAC maximum within each cell.

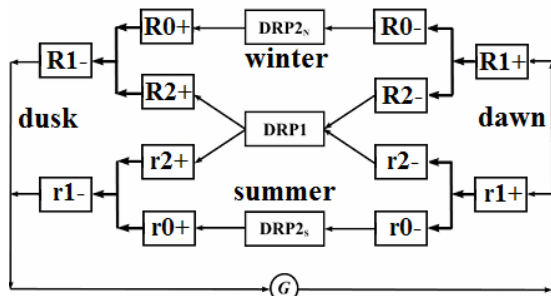


**Figure 2.** Scheme of the M-I system electric circuit for two hemispheres. Explanations are provided in the text.

Further, the current flows from DRP1 into the ionosphere of both hemispheres and closes onto the generator through the R1-and r1-cells. The letter  $r$  replaces the letter  $R$  in the Southern Hemisphere. Now, we switch to the  $I_{RN\pm}$  intensity plots in each of the  $RN\pm$  cells in the Northern Hemisphere. Fig. 3 presents the plots from the data on the 2000 April 6 (02-04) UT interval. The plots are grouped by the Kirchhoff Rule 1. In the Northern Hemisphere, the following equations correspond to this rule

$$I_{R1+} = (I_{R2+}) + (I_{R0-}) \quad (1)$$

$$I_{R1-} = (I_{R2+}) + (I_{R0+}) \quad (2)$$

Here, Equations (1) and (2) are for the postmidnight (‘‘dawn’’) and premidnight sector (‘‘dusk’’) of the MLT nightside half. In the Southern Hemisphere, the same equations, but with the letter  $r$  instead of the letter  $R$  are true. The cell boundary was determined in one of the R1 nightside sectors, the boundaries of the corresponding nightside cells in R2 and R0 were determined through fitting based on Equations (1), (2) (within 10-20%). Further, there follow the technique applications.

Now, we analyze the FAC behavior during two intervals of the 6 April 2000 superstorm. Fig. 5 (Appendix) provides the variations in the SW parameters and AE indices.

### 3. Events 1, (02-03) UT interval

Fig. 3 presents the first maximum of AE index at 0255 UT, and, simultaneously, the FAC intensity maximum in the R1-, R2+ cells of the dusk sector. In contrast, the minimum of the  $I_{R1+}$ ,  $I_{R2-}$  values is observed at the same time in the dawn sector. Such a FAC distribution corresponds to the EP summer-type FAC in the Northern Hemisphere [Mishin et al., 2015a].

### 4. Events 2, (03-04) UT interval

Fig. 3 also presents the AE index second maximum at 0335 UT, and, simultaneously, the FAC intensity maximum in R1+ and R2- cells of the dawn sector. In contrast, one observes the  $I_{R1-}$  and  $I_{R2+}$  minimum in the dusk sector at the same time. Such a FAC distribution corresponds to the EP winter-type FAC in the Northern Hemisphere [Mishin et al., 2015b].

### 5. Events 3, (12-15) UT interval

In Fig. 4, one can see the AE index first maximum at 1330 UT, and, simultaneously, the FAC intensity maximum in the R1-, R2+ cells of the dusk sector. In contrast, one observes low values of  $I_{R1+}$ ,  $I_{R2-}$  in the dawn sector at the same time. Such a FAC distribution corresponds to the EP summer-type FAC in the Northern Hemisphere [Mishin et al., 2015a].

## 6. Discussion and Conclusions

We addressed three intervals with signatures of separate expansion phases (EPs) during the 2000 April 6

superstorm. For each of them, the plots of variation in the FAC intensity in the cells of premidnight and postmidnight sectors of each of three Iijima and Potemra Regions were obtained. On such a basis, we showed that, during the equinox season, one observes two EP types detected recently, and termed "EP summer type" and "EP winter type" [Mishin et al., 2015]. Within the latter, the FAC space distribution and dynamics during EP differ dramatically. We offer a scenario, in which the winter-type EP starts with the collapse (decrease) of FAC that downflows into the ionosphere of the winter hemisphere in the R1 premidnight sector. Simultaneously, and with almost at the same rate, there occurs the FAC increase in the adjacent R1 postmidnight sector. Thus, in the proposed scenario, the substorm EP starts simultaneously in two hemispheres, but in different MLT sectors of the nightside I-P Region 1. The M-I feedback instability in the premidnight sector of the summer hemisphere serves as an initiator and organizer of the global EP (see, e.g., [Atkinson, 1970]).

**Acknowledgements.** We thank the ISTP SB RAS MIT group members and Dr. E.V. Mishin for stimulating discussions. The AE index was obtained from the World Data Center for Geomagnetism, Kyoto. We are grateful to PIs of the CANOPUS, INTERMAGNET, GIMA, MACCS, IMAGE projects and of magnetic networks in Arctic and the Antarctic (the Shafer Institute of Cosmo-Physical Research and Aeronomy SB RAS, Arctic and Antarctic Research Institute, and DMI), and individual magnetic observatories for providing magnetic data used in this study. Work was supported by the RFBR under Grants 14-05-91165 and 15-05-05561. C. and J.Y. Wang are supported by NSFC Grant 413111039.

## References

- Akasofu SI (2013) The relationship between the magnetosphere and magnetospheric/auroral substorms. *Ann Geophys* 31 (3):387-394. doi:10.5194/angeo-31-387-2013
- Atkinson G (1970) Auroral arcs: Result of the interaction of a dynamic magnetosphere with the ionosphere. *J Geophys Res* 75 (25):4746-4755. doi:10.1029/JA075i025p04746
- Anderson BJ, Korth H, Waters CL, Green DL, Merkin VG, Barnes RJ, Dyrud LP (2014) Development of large-scale Birkeland currents determined from the Active Magnetosphere and Planetary Electrodynamics Response Experiment. *Geophys Res Lett* 41 (9):2014GL059941. doi:10.1002/2014gl059941
- Cowley SWH (2000) Magnetosphere-ionosphere interactions: A tutorial review. In: Magnetospheric Current Systems, vol 118. *Geophys. Monogr. Ser. AGU*, Washington, DC, pp 91-106. doi:10.1029/GM118p0091
- Kabin K, Rankin R, Rostoker G, Marchand R, Rae JJ, Ridley AJ, Gombosi TI, Clauer CR, DeZeeuw DL (2004) Open-closed field line boundary position: A parametric study using an MHD model. *J Geophys Res* 109. doi:10.1029/2003ja010168
- Kamide Y, Baumjohann W (1993) Magnetosphere-ionosphere coupling. Springer-Verlag, Berlin
- Korth H, Rastatter L, Anderson BJ, Ridley AJ (2011) Comparison of the observed dependence of large-scale Birkeland currents on solar wind parameters with that obtained from global simulations. *Ann Geophys* 29 (10):1809-1826. doi:10.5194/angeo-29-1809-2011
- Laundal KM, Østgaard N (2009) Asymmetric auroral intensities in the Earth's Northern and Southern hemispheres. *Nature* 460 (7254):491-493. doi:10.1038/nature08154
- Lyatsky WB, Maltsev YP, Leontyev SV (1974) Three-dimensional current system in different phases of a substorm. *Planet Space Sci* 22 (8):1231-1247. doi:10.1016/0032-0633(74)90007-5
- Lui ATY, Kamide Y (2003) A fresh perspective of the substorm current system and its dynamo. *Geophys Res Lett* 30 (18):1958. doi:10.1029/2003gl017835

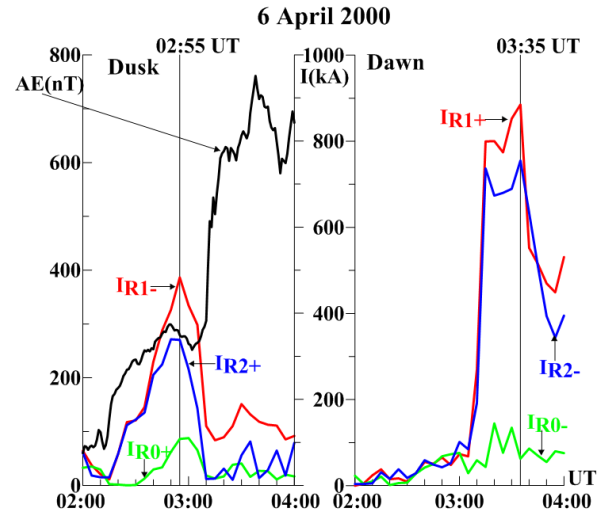


**Figure 3.** Variations in the FAC intensities in cells of three I-P Regions in the premidnight (dusk) and postmidnight (dawn) sectors. Vertical lines mark the EP maximum time for Event 1 (0255 UT) and Event 2 (0355 UT). Also, the AE index plot is provided. Event 1 is at (02±03) UT. Event 2 – at (03±04) UT.

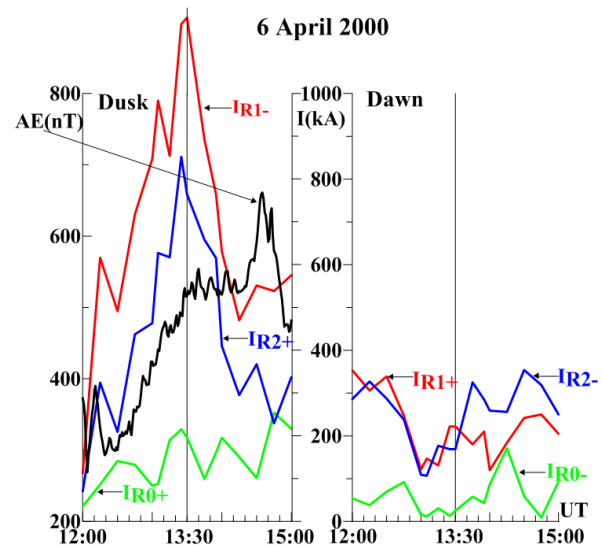


**Figure 4.** Event 3 within the 12–15 UT interval. The designations are the same as those in Fig. 3

- McPherron RL, Russell CT, Aubrey MP (1973) Satellite studies of magnetospheric substorms on August 15, 1968: 9. Phenomenological model for substorms. *J Geophys Res* 78 (16):3131-3149. doi:10.1029/JA078i016p03131
- Mishin VM, Lunyushkin SB, Shirapov DS, Baumjohann W (1986) A new method for generating instantaneous ionospheric conductivity models using ground-based magnetic data. *Planet Space Sci* 34 (8):713-722. doi:10.1016/0032-0633(86)90125-x
- Mishin VM (1990) The magnetogram inversion technique and some applications. *Space Sci Rev* 53 (1):83-163. doi:10.1007/bf00217429
- Mishin VM, Karavaev YA, Sapronova LA, Solovyev SI (2012) Activation of the tail open part during the magnetospheric storm. *Cosmic Res* 50 (4):272-281. doi:10.1134/s001095251204003x
- Mishin VM, Förster M, Kurikalova MA, Mishin VV (2011) The generator system of field-aligned currents during the April 06, 2000, superstorm. *Adv Space Res* 48 (7):1172-1183.
- Mishin VV et al (2015a) Positive feedback between ionosphere conductivity and field-aligned current intensity// *Earth Planets Space* (submitted)
- Mishin VV et al (2015b) Versions of model for the solar wind-magnetosphere-ionosphere global electric circuit in substorms of summer and winter seasons// *Earth Planets Space* (submitted)
- Ohtani S, Wing S, Merkin VG, Higuchi T (2014) Solar cycle dependence of nightside field-aligned currents: Effects of dayside ionospheric conductivity on the solar wind-magnetosphere-ionosphere coupling. *J Geophys Res Space Physics* 119 (1):322-334. doi:10.1002/2013ja019410
- Østgaard N, Humeret BK, Laundal KM (2011) Evolution of auroral asymmetries in the conjugate hemispheres during two substorms. *Geophys Res Lett* 38 (3):L03101. doi:10.1029/2010gl046057
- Papitashvili VO, Christiansen F, Neubert T (2002) A new model of field-aligned currents derived from high-precision satellite magnetic field data. *Geophys Res Lett* 29 (14):1683. doi:10.1029/2001gl014207
- Reistad JP, Østgaard N, Laundal KM, Haaland S, Tenfjord P, Snekvik K, Oksavik K, Milan SE (2014) Intensity asymmetries in the dusk sector of the poleward auroral oval due to IMFBx. *J Geophys Res Space Physics* 119 (12):9497-9507. doi:10.1002/2014ja020216
- Sandholz PE, Farrugia CJ, Denig WF (2014) M-I coupling across the auroral oval at dusk and midnight. *Ann Geophys* 32 (4):333-351. doi:10.5194/angeo-32-333-2014
- Shirapov DS, Mishin VM, Bazarzhapov AD, Saifudinova TI (2000) Adapted dynamic model of ionospheric conductivity. *Geomagnetism and Aeronomy* 40 (4):471-475
- Siscoe GL (1982) Energy Coupling Between Regions 1 and 2 Birkeland Current Systems. *J Geophys Res* 87 (A7):5124-5130. doi:10.1029/JA087iA07p05124
- Sofko GJ, McWilliams KA, Bryant CR (2013) The substorm current wedge and midnight sector partial ring current near substorm onset. *Adv Polar Sci* 24 (1):32-41. doi:10.3724/SP.J.1085.2013.00032
- Sugiura M (1975) Identifications of the polar cap boundary and the auroral belt in the high-altitude magnetosphere: A model for field-aligned currents. *J Geophys Res* 80 (16):2057-2068. doi:10.1029/JA080i016p02057
- Weimer DR (2001) Maps of ionospheric field-aligned currents as a function of the interplanetary magnetic field derived from Dynamics Explorer 2 data. *J Geophys Res* 106 (A7):12889-12902. doi:10.1029/2000ja00029

## Application

6 April 2000

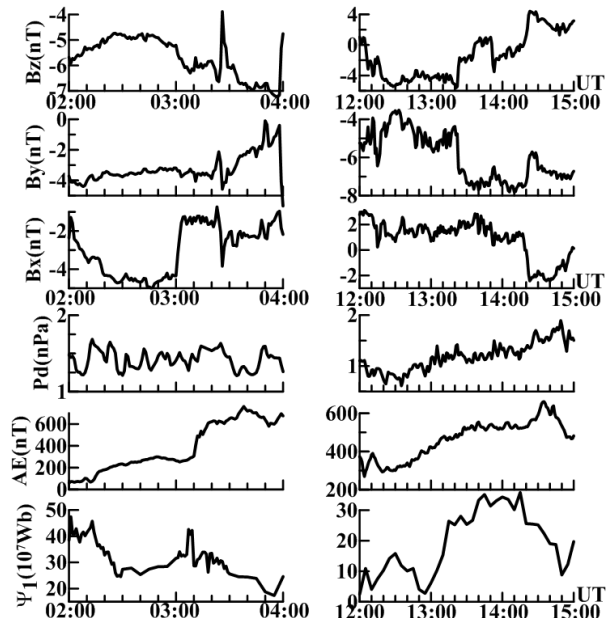


**Figure 5.** Two intervals under study, variations of the IMF components ( $B_x$ ,  $B_y$ ,  $B_z$ ), the SW dynamic pressure ( $P_d$ ), AE indexes and the “new” polar cap magnetic flux  $\Psi_1 = \Psi - \Psi_0$  ( $\Psi$ - the total flux,  $\Psi_0$ -its value before substorm –see in [Mishin et al., 2014]).